Steel and Composite Structures, *Vol. 35, No. 2 (2020) 279-294*
DOI: https://doi.org/10.12989/scs.2020.35.2.279

Effect of progressive shear punch of a foundation on a reinforced concrete building behavior

Morteza Naghipour[1], Kia Moghaddas Niak[1],
Mahdi Shariati[*2,3] and Ali Toghroli[4]

[1]Department of Civil Engineering, Babol Noshirvani University of Technology, Babol, Iran
[2]Division of Computational Mathematics and Engineering, Institute for Computational Science, Ton Duc Thang University, Ho Chi Minh City 758307, Vietnam
[3]Faculty of Civil Engineering, Ton Duc Thang University, Ho Chi Minh City 758307, Vietnam
[4]Institute of Research and Development, Duy Tan University, Da Nang 550000, Vietnam

(*Received July 24, 2019, Revised March 22, 2020, Accepted March 25, 2020*)

Abstract. Foundation of a building is damaged under service loads during construction. First visit shows that the foundation has been punched at the 6 column's foot region led to building rotation. Foundation shear punching occurring has made some stresses and deflections in construction. In this study, progressing of damage caused by foundation shear punching and inverse loading in order to resolve the building rotation has been evaluated in the foundation and frame of building by finite element modeling in ABAQUS software. The stress values of bars in punched regions of foundation has been deeply exceeded from steel yielding strength and experienced large displacement based on software's results. On the other hand, the values of created stresses in the frame are not too big to make serious damage. In the beams and columns of ground floor, some partial cracks has been occurred and in other floors, the values of stresses are in the elastic zone of materials. Finally, by inverse loading to the frame, the horizontal displacement of floors has been resolved and the values of stresses in frame has been significantly reduced.

Keywords: shear punching; foundation; progressive collapse; inverse loading; ABAQUS

1. Introduction

Due to the whole load (vertical and lateral) transferring to the ground, foundation is one of the most important structural parts in buildings. During foundation design, two kinds of shear strength must be controlled as slabs, flexural shear and punching shear. Flexural shear or one-way shear causes diagonal cracks and probable fracture which can propagate throw the whole structures. The critical section in one-way shear is the section in distance of d from column side and parallel to it (d is the effective depth of foundation). Punching shear or two-way shear tends to make diagonal cracks and foundation fracture around a column. Indeed, creation of peripheral forces in connection of column and foundation regions is the result of transferring vertical load from column to foundation. These peripheral forces lead the foundation to fracture in frustum shape in the connection zone. The angle of crack line in punching shear with the horizontal axis is assumed about 45o. Therefore, it is inferable that the critical section is the vertical section in distance d/2 from column side and parallel to it (Fig. 1) (Mc Cormac 2001, MacGregor 2002). In two-way action, foundation must tolerate the shear force in two directions of the region around the concentrated load, based on ACI code. In this action, the critical section is the lateral surface of a prism which is perpendicular to foundation surface. This section is in distance d/2 from every edges and sides of load effect section. The critical section should be considered in a way that the perimeter of polygon became minimal. Critical perimeters around the columns are shown in Fig 1 (Mc Cormac 2001, MacGregor 2002).

ACI code suggests the capacity of punching shear section by the minimum value of following relations

$$V_c = \min \begin{cases} \left(1+\dfrac{2}{\beta}\right)\dfrac{\sqrt{f'_c}}{3} b_0 d \\ \left(\dfrac{\alpha_s d}{b_0}+1\right)\dfrac{\sqrt{f'_c}}{12} b_0 d \\ \dfrac{\sqrt{f'_c}}{3} b_0 d \end{cases} \tag{1}$$

Where b_0 is the perimeter of polygon, d is the effective depth of foundation, f'_c is the compressive strength of concrete, β is the ratio of length over width of column section and α_s is a factor which is 40 for a central column, 30 for a side column and 20 for an edge column (ACI 318-05 2005).

2. Case study model

A six-storey reinforced concrete building has been damaged during the last phases of construction process in Babol. Site first visits have shown that the mat foundation

∗Corresponding author, Ph.D.
E-mail: shariati@tdtu.edu.vn

http://www.techno-press.org/?journal=scs&subpage=8
ISSN: 1229-9367 (Print), 1598-6233 (Online)

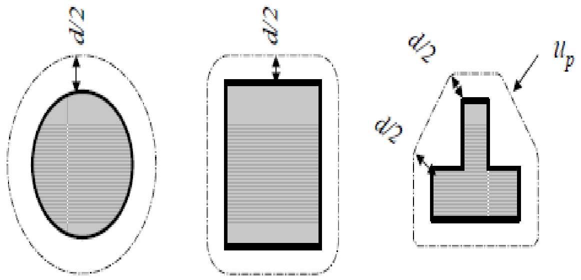

Fig. 1 Perimeter of the critical section

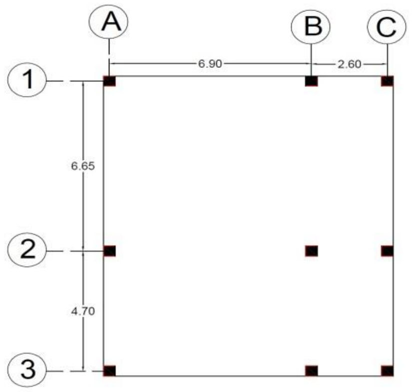

Fig. 2 Foundation of building and the place of columns

Fig. 3 Rotation of building caused by foundation shear punch

of building in Fig. 2 has been punched at the regions of six columns (3 columns of A axis and 3 columns of B axis). Displacement of A axis columns has been reported about 20 cm and 5 cm for B axis's columns. Punching shear occurring is an asymmetric subsidence for the building and rotate it to one side and pretended that the building is overturning (Fig. 3).

There are some essential differences between the executed foundation and its designed plan such as thickness of foundation designed 70 cm and under the side columns 90 cm, but constructed 60 cm thickness. In northern and southern sides of foundation of plans, there are heels with a length of 110 cm, while in the western and eastern sides with a length of 20 cm and 10 cm, all these heels are removed during the constructing process. In design process, the compressive strength of foundation concrete is *210* kg/cm^2, but the compressive strength of constructed foundation concrete is reported *85* kg/cm^2 based on the experimental result. Table 1 has shown the differences between the constructed frame of building and the element's sizes in the plans.

Composite floor systems which are containing interconnected steel beam and concrete slab have a suitable interaction and withstand against the flexural and compressive stress; however, the possible shear force is always threatening the steel-concrete interlock. Whereas the steel-concrete interlocking system requires an improvement, some researchers proposed shear connectors to enhance the shear resistivity of the composite systems. Shear connectors are mainly used in steel-concrete composite systems to establish a connection through which the developed shear forces at the interface of the materials can be collected and transferred. In composite beams with partial interaction, a specific number of shear connectors are employed along the length of beams, and these connectors primarily control the behavior of the beams under different loading conditions. Besides, the load-bearing capacity, stiffness, and ductility of connectors highly affect the applicable theories in order to analyze the floor systems. This concept could be followed in the shallow foundations or other structures faced with shear forces. Employing typical C-shaped or stud shear connectors in foundations could be useful, and researchers can also design new types of shear connectors to perform better in foundations (Shariati *et al.* 2011, Shariati *et al.* 2012, Shariati 2013, Mohammadhassani *et al.* 2014, Khorramian *et al.* 2016, Shahabi *et al.* 2016, Tahmasbi *et al.* 2016, Shariati *et al.* 2017, Hosseinpour *et al.* 2018, Nasrollahi *et al.* 2018, Paknahad *et al.* 2018, Wei *et al.* 2018, Davoodnabi *et al.* 2019).

Concrete has outstanding compressive strength due to its dense and robust texture which does not experience the local or distortional buckling or other accidental deformations along with low flexural and tensional strength. These features make concrete to be useful material for columns and axial structural elements. Concrete has also been cast in different shapes and types, which self-consolidating, porous, high strength, lightweight, and green concrete are the most applicable ones. Moreover, concrete members are expanded due to Poisson's effect under axial pressure. Therefore, as a brittle material, the general fracture occurs in concrete members when the stress reaches the ultimate limit. Fresh and hardened properties are two types of significant characteristics of concrete. Fresh properties include the most primitive properties of concrete, such as slump and workability. On the contrary, hardened properties contain critical features such as compressive strength, flexural strength, shear strength, and corrosion resistance. In recent years, different attempts have been conducted to enhance these properties such as surface protection, the inclusion of the fibres and cementitious replacement powders (Sinaei *et al.* 2011, Toghroli *et al.* 2017, Ismail *et al.* 2018, Nosrati *et al.* 2018, Toghroli *et al.* 2018, Ziaei-Nia *et al.* 2018, Davoodnabi *et al.* 2019, Li *et al.* 2019, Luo *et al.* 2019, Sajedi *et al.* 2019, Shariati *et al.* 2019a, Shariati *et al.* 2019b, Suhatril *et al.* 2019, Trung *et al.* 2019, Xie *et al.* 2019, Naghipour *et al.* 2020).

In this study, the building's foundation, frame and all their reinforcement bars have been modeled by finite element software ABAQUS. During the modeling process, it is tried that dimensions of foundation and concrete frame, numbers and lengths of the bars, models of materials, boundary conditions and loading are defined as the constructed building conditions in order to achieve acceptable results.

3. Discussion and investigation

3.1 Modeling process

In order to create the model of building, only the structural elements have been modeled in 3 different parts which are named frame (beams and columns), foundation and bars. Parts of the frame and foundation are modeled as the solid parts and bars as wire. In property module, materials has been defined and assigned to the parts. Concrete damage plasticity (CDP) (Abaqus analysis user's manual 2009) model has been used to define the foundation concrete in order to model the punching shear fracture and damage.

3.1.1 Concrete damage plasticity (CDP)

CDP model used in ABAQUS software is a modification of Drucker–Prager strength hypothesis. In recent years, the latter has been further modified by Lubliner (1989), Lee (1998) and Fenves. According to the modifications, the failure surface in deviator cross section needs not to be a circle and governed by parameter K_C. Physically, parameter K_C is interpreted as a ratio of distances between the hydrostatic axis and respectively the compression meridian and the tension meridian in deviator cross section. This ratio is always higher than 0.5.

While this value is 1, the deviator cross section of the failure surface becomes a circle (as in the classic Drucker–Prager strength hypothesis). CDP model recommends to assume $K_C = 2/3$. This shape is similar to the strength criterion (a combination of three mutually tangent ellipses) formulated by William (1975) and (Li *et al.* 2015). It is a theoretical experimental criterion based on triaxial stress test results (Fig. 4.). Similarly, the shape of the plane's meridians in stress space changes the experimental results, indicating that the meridians are curves. In CDP model, the plastic potential surface in the meridional plane assumes the form of a hyperbola. The shape is adjusted through eccentricity (plastic potential eccentricity). It is a small positive value which expresses the rate of approach of plastic potential hyperbola to its asymptote. In other words, it is the length (measured along the hydrostatic axis) of the segment between the vertex of hyperbola and the intersection of asymptotes of this hyperbola (the center of the hyperbola). Parameter eccentricity can be calculated as a ratio of tensile strength to compressive strength. CDP model recommends to assume $\epsilon = 0.1$. When $\epsilon = 0$, the surface in meridional plane becomes a straight line (the classic Drucker-Prager hypothesis) (Fig. 5) (Torres 2015, Jankowiak 2008). Another parameter describing the state of the material is the point in which the concrete undergoes a failure under biaxial compression. σb0/σC0 (fb0/fc0) is the ratio of strength in biaxial state to the strength in uniaxial state. Accordingly, the most reliable is the experimental results reported by Kupler in 1969 (Torres 2015, Jankowiak 2008). After their approximation with the elliptic equation, uniform biaxial compression strength fCC is equal to $1.16248 f_{c0}$. ABAQUS user-manual specifies default σ_{b0}/σ_{c0} =1.16 (Fig. 6). Last parameter characterizing the performance of concrete under compound stress is dilation angle, i.e., the angle of inclination of failure surface towards the hydrostatic axis measured in meridional plane. Physically, dilation angle ψ is interpreted as a concrete internal friction angle. In simulations, usually $\psi = 36°$or $\psi= 40°$ is assumed.

Unquestionable advantage of CDP model is the fact that it is based on parameters with an explicit physical interpretation. The exact role of the above parameters and the mathematical methods used to describe the development of boundary surface in a three-dimensional space of stresses are explained in ABAQUS user-manual. Other parameters describing the performance of concrete are determined for uniaxial stress. Table 2 shows the model's parameters, characterizing its performance under compound stress.

Table 1 Beams and column differences between the constructed frame and designed plans

Beams and columns of the floors	Constructed sections sizes (cm^2)	Sections sizes in the designed plans (cm^2)
Ground floor	50X50	55X55
1th floor	45X45	55X55
2th floor	45X45	50X50
3th floor	40X40	50X50
4th floor	40X40	45X45
5th floor	40X40	45X45

Table 2 Default parameters of CDP model under compound stress

Parameter name	Value
Dilation angle	36°
Eccentricity	0.1
f_b^0/f_c^0	1.16
K	0.667
Viscosity parameter	0.0001

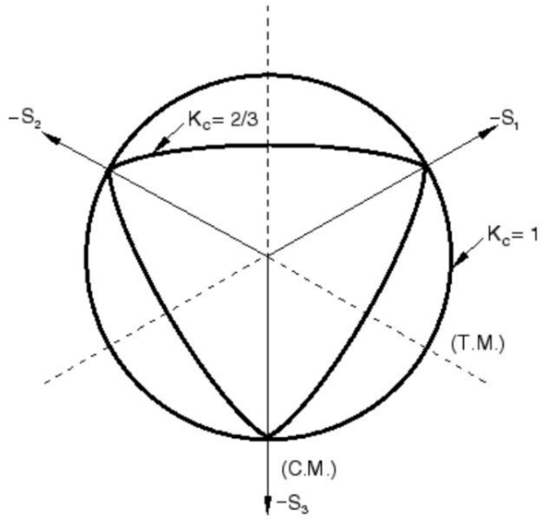

Fig. 4 Deviatoric cross section of failure surface in CDP model

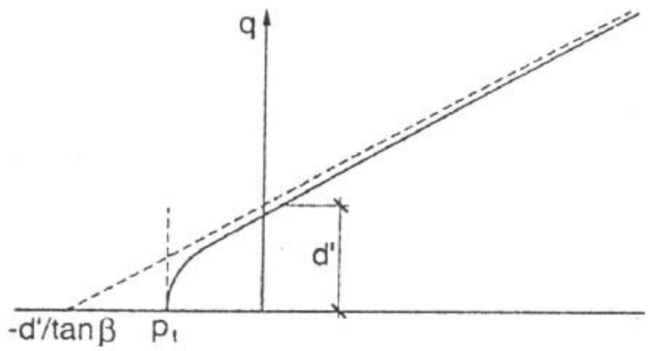

Fig. 5 Hyperbolic surface of plastic potential in meridional plane

3.1.2 Stress-strain curve for uniaxial compression

The stress strain relation for a given concrete can be accurately described on the basis of uniaxial compression test which is carried out on it. Regarding the graph of laboratory test, variables should be transformed. Inelastic strains $\tilde{\varepsilon}_c^{in}$ are used in CDP model. In order to determine them, the elastic part should be deducted (corresponding to the undamaged material) from the total strains registered in uniaxial compression test (Fig. 7) (Bao 2008).

$$\tilde{\varepsilon}_c^{in} = \varepsilon_c - \varepsilon_{0c}^{el} \quad (2)$$

$$\varepsilon_{0c}^{el} = \frac{\sigma_c}{E_0} \quad (3)$$

While transforming strains, the moment on which the material should be defined as nonlinearly elastic should be considered. Although uniaxial tests show that this behavior could occur almost from the beginning of compression process, for most numerical analyses, it can be neglected in the initial stage. According to Majewski (2003), a linear elasticity limit should be increased with concrete strength and it should be assumed rather than the one experimentally determined, resulting that it as a percentage of stress to concrete strength from this formula

$$e_{lim} = 1 - \exp\left(\frac{-f_c}{80}\right) \quad (4)$$

This ceiling can be simply arbitrarily assumed as $0.4f_{cm}$. Eurocode 2 specifies the modulus of elasticity for concrete to be secant in a range of 0–0.4 f_{cm}. Since the basic definition of material has already covered the shear modulus and longitudinal modulus of concrete, at this stage, it is good to assume such an inelastic phase threshold that the initial value of Young's modulus and the secant value determined based on the standard would be convergent. In most numerical analyses, it is rather not the initial behavior of material, but the stage in which it reaches its yield strength while investigated to the level of $0.4f_{cm}$, there are fewer problems with solution convergence. Defining the yield stress-inelastic strain pair of variables, degradation variable d_c should be defined and ranged from 0 for an undamaged material to 1 for the total loss of load-bearing capacity. These values can also be obtained from the uniaxial compression tests by calculating the ratio of stress for declining part of curve to the compressive strength of concrete. Respectively, CDP model allows the calculation of plastic strain from this formula

$$\tilde{\varepsilon}_c^{pl} = \varepsilon_c^{in} - \frac{d_c}{(1-d_c)}\frac{\sigma_c}{E_0} \quad (5)$$

Where E_0 stands as the initial modulus of elasticity for undamaged material. Knowing the plastic strain and determining the flow and failure surface area, stress σ_c for uniaxial compression and its effective stress $\bar{\sigma}_c$ could be calculated

$$\sigma_c = (1-d_c)E_0(\varepsilon_c - \tilde{\varepsilon}_c^{pl}) \quad (6)$$

$$\bar{\sigma}_c = \frac{\sigma_c}{(1-d_c)} = E_0(\varepsilon_c - \tilde{\varepsilon}_c^{pl}) \quad (7)$$

3.1.3 Stress – strain curve for uniaxial tension

Tensile strength of concrete under uniaxial stress is rarely determined through a direct tension test because of the difficulties involved in its execution and the large scatter of results. Indirect methods such as sample splitting or beam bending tend to be used

$$F_{ctm} = 0.3f_{ck}^{(2/3)} \quad (8)$$

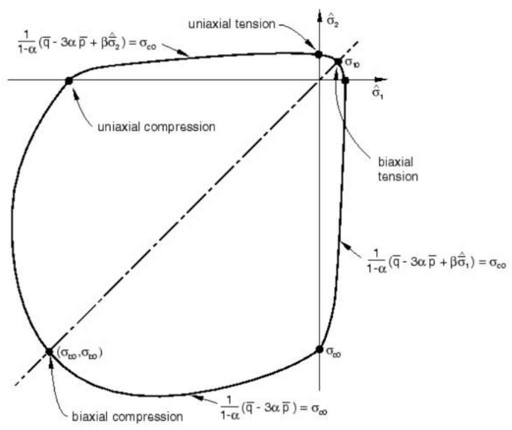

Fig. 6 Strength of concrete under biaxial stress in CDP model

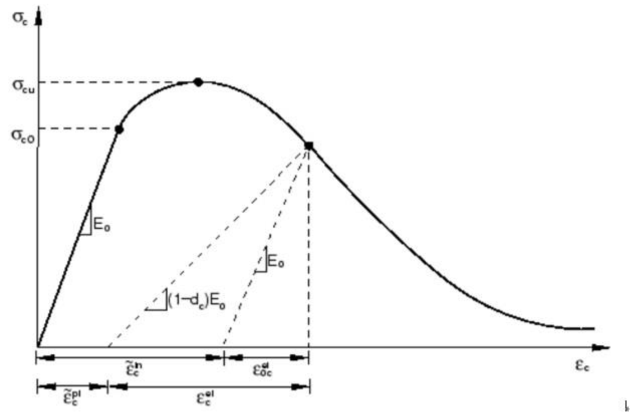

Fig. 7 Definition of inelastic strain

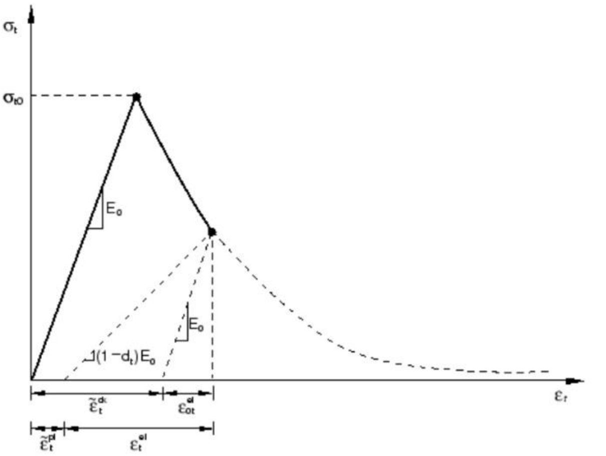

Fig. 8 Definition of strain after cracking – tension stiffening

The term cracking strain $\tilde{\varepsilon}_t^{ck}$ is used in CDP model numerical analysis. The aim is to consider the phenomenon called tension stiffening. Concrete under tension is not regarded as a brittle-elastic body and such phenomena as aggregate that is interlocked in a crack and concrete-to-steel adhesive between cracks are taken into account. This assumption is valid when the pattern of cracks is fuzzy. Thus, the stress in tensioned zone has been gradually decreased. The strain after cracking is defined as a difference between total strain and elastic strain for undamaged material

$$\tilde{\varepsilon}_t^{ck} = \varepsilon_t - \varepsilon_{0t}^{el} \tag{9}$$

$$\varepsilon_{0t}^{el} = \frac{\varepsilon_t}{E_c} \tag{10}$$

Plastic strain $\tilde{\varepsilon}_t^{pl}$ is calculated similarly as the case of compression after defining degradation parameter d_t and calculated based on the stress-strain curves for uniaxial tension (Fig. 8).

3.1.4 Plotting stress-strain curve without detailed laboratory test results

On the basis of uniaxial compression test results, how the material behave should be accurately determined. However, problem arises when there is no test results on running such a numerical simulation or when the analysis is performed for a new structure. Then the only available quantity is the average compressive strength (*fcm*) of concrete. Another quantity known to begin an analysis of stress-strain curve is the longitudinal modulus of elasticity (*Ecm*) of concrete. Its value can be calculated by using the relations available in literature

$$E_{cm} = 22(0.1f_{cm})^{0.3} \tag{11}$$

Where f_{cm} and E_{cm} are GPa.

Other values defining the location of characteristic points on the graph are strain ε_{c1} at average compressive strength and ultimate strain ε_{cu}

$$\varepsilon_{c1} = 0.7(f_{cm})^{0.31} \tag{12}$$

$$\varepsilon = 3.5\% \tag{13}$$

On the basis of experimental results, Majewski (2003) has proposed the following (quite accurate) approximating formulas

$$\varepsilon_{c1} = 0.0014[2 - exp(- 0.024 f_{cm}) - exp(- 0.140 f_{cm})] \tag{14}$$

$$\varepsilon_{cu} = 0.004 - 0.0011[1 - exp(- 0.0215 f_{cm})] \tag{15}$$

By knowing the values of the above, the points which the graph should intersect can be determined (Fig. 9).

The most popular formulas are presented in Table 3, however, the original symbols are replaced with the uniform denotations used in Eurocode 2 (2004). Choosing a proper formula form to describe the relation $\sigma_c - \varepsilon_c$, the longitudinal modulus of elasticity mightily represents the initial value E_c (at stress $\sigma_c = 0$) or secant modulus E_{cm}. Most of the formulas use the initial modulus E_c which is neither experimentally determined nor taken from the standards. Another important factor is the functional dependence itself. This function is not adequately flexible to properly describe the performance of concrete (Murthy 2015).

The 2nd order parabola has this property that the tangent of angle of a tangent passing through a point on its branch relatively measured to the horizontal axis passing through this point is always double to the angle measured as the inclination of secant passing through the same point and extremum of parabola, relative to the same horizontal axis (Fig. 10) (Muttoni 2008).

The consequence of this property of parabola is either the exceedance of the concrete's strength for a correct initial modulus value or the necessity to lower the value in order to reach a specific stress value in the extreme. Fig. 11 shows the relation $\sigma_c - \varepsilon_c$ for Madrid parabola in grade C16/20 concrete. The following batch denotations are assumed

- $E_{cm} - E_c = E_{cm}$ = 28608 MPa is assumed as the initial modulus and calculate extremum f_{cm} = 26.81 MPa,
- E_c/E_{cu} = 2 doubled tangent of the secant angle passing through the point (ε_{c1}, f_{cm}), amounting to E_c = 25602 MPa and calculate extremum f_{cm} = 24 MPa (correct),

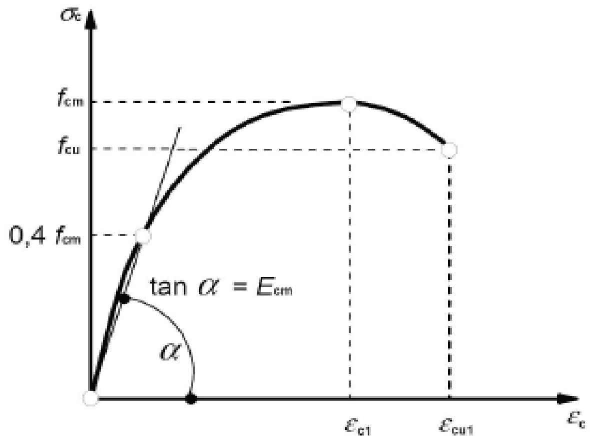

Fig. 9 Stress-strain diagram for analysis of structures (Eurocode 2 2004)

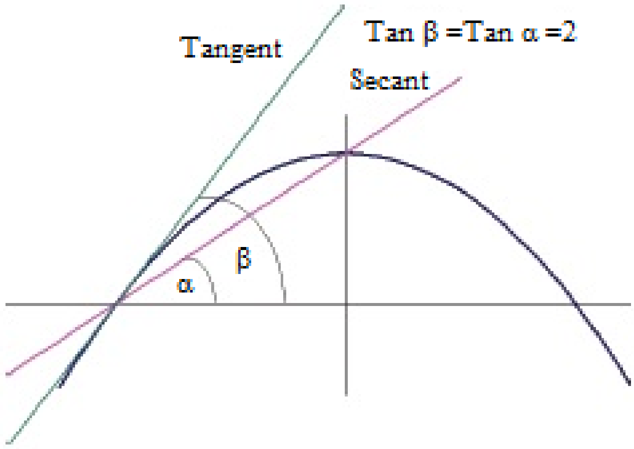

Fig. 10 Property of second order parabola (Eurocode 2, 2004)

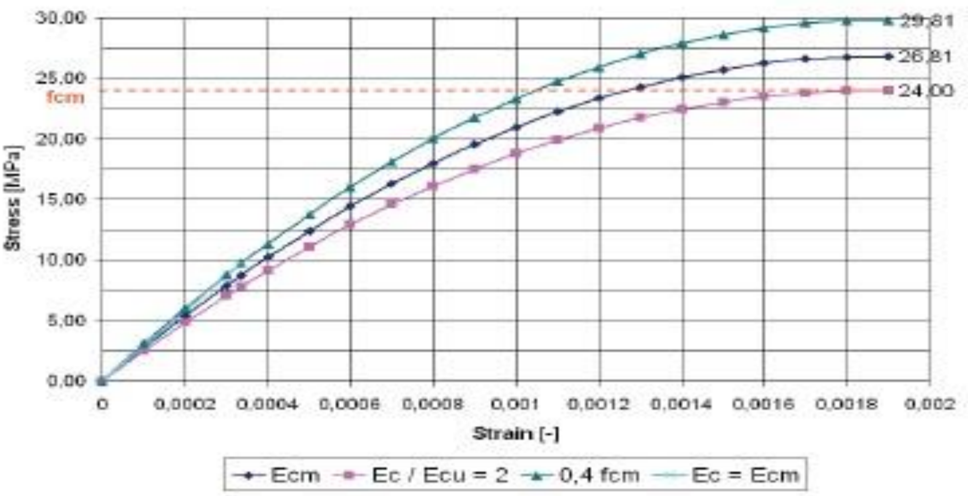

Fig. 11 Relation σc-εc for Madrid parabola depending on longitudinal modulus of elasticity (Eurocode 2, 2004)

0.4 f_{cm} – the value of initial modulus E_c = 31808 MPa is matched so that the curve intersects point (ε_c, 0.4f_{cm}), calculate extremum f_c = 29.81 MPa.

When the initial modulus E_c is assumed to amount E_{cm}, the strength of concrete is much overrated, despite the fact that, the initial modulus is still underrated (numerically E_{cm} is not the highest value). In the case of parabolic relations, the

Table3 Most popular formulas for stress-strain of concrete

Formula name/ Source	Formula form	Variables
Madrid parabola	$\sigma_c = E_c\varepsilon_c[1-\frac{1}{2}(\frac{\varepsilon_c}{\varepsilon_{c1}})]$	$\sigma_c = f(E_c,\ \varepsilon_{c1})$
Desay & Krishnan Formul (Xiao 2000)	$\sigma_c = \frac{E_c\varepsilon_c}{1+(\frac{\varepsilon_c}{\varepsilon_{c1}})}$	$\sigma_c = f(E_c,\ \varepsilon_{c1})$
EN 1992-1-1	$\sigma_c = f_{cm}\frac{k\eta-\eta^2}{1+(k-2)\eta}$ $k=1.05E_{cm}\frac{\varepsilon_{c1}}{f_{cm}}$, $\eta = \frac{\varepsilon_c}{\varepsilon_{c1}}$	$\sigma_c = f(E_{cm}, f_{cm},\ \varepsilon_{c1})$
Majewski Formula (Majewski 2003)	$\sigma_c = E_c\varepsilon_c$ if $\sigma_c \leq e_{lim}f_{cm}$ $\sigma_c = f_{cm}\frac{(e_{lim}-2)^2}{4(e_{lim}-1)}(\frac{\varepsilon_c}{\varepsilon_{c1}})^2 + f_{cm}\frac{(e_{lim}-2)^2}{2(e_{lim}-1)}(\frac{\varepsilon_c}{\varepsilon_{c1}}) + f_{cm}\frac{e_{lim}^2}{4(e_{lim}-1)}$ $E_c = \frac{f_{cm}}{\varepsilon_c}(2-e_{lim})$, if $\sigma_c \geq e_{lim}f_{cm}$	$\sigma_c = f(E_c, f_{cm},\ \varepsilon_{c1})$
Wang and Hsu Formula (Wang 2001)	$\sigma_c = \zeta f_{cm}[2(\frac{\varepsilon_c}{\zeta\varepsilon_{c1}}) - (\frac{\varepsilon_c}{\zeta\varepsilon_{c1}})^2]$ if $\frac{\varepsilon_c}{\zeta\varepsilon_{c1}} \leq 1$ $\sigma_c = \zeta f_{cm}[1-(\frac{\frac{\varepsilon_c}{\zeta\varepsilon_{c1}}-1}{\frac{2}{\zeta}-1})^2]$ if $\frac{\varepsilon_c}{\zeta\varepsilon_{c1}} \geq 1$	$\sigma_c = f(f_{cm},\ \varepsilon_{c1})$
Sáenz formula (Sasani 2008)	$\sigma_c = \frac{\varepsilon_c}{A+B\varepsilon_c+C\varepsilon_c^2+D\varepsilon_c^3}$	$\sigma_c = f(E_c, f_{cm}, f_{cu},\ \varepsilon_{c1},\ \varepsilon_{cu1})$

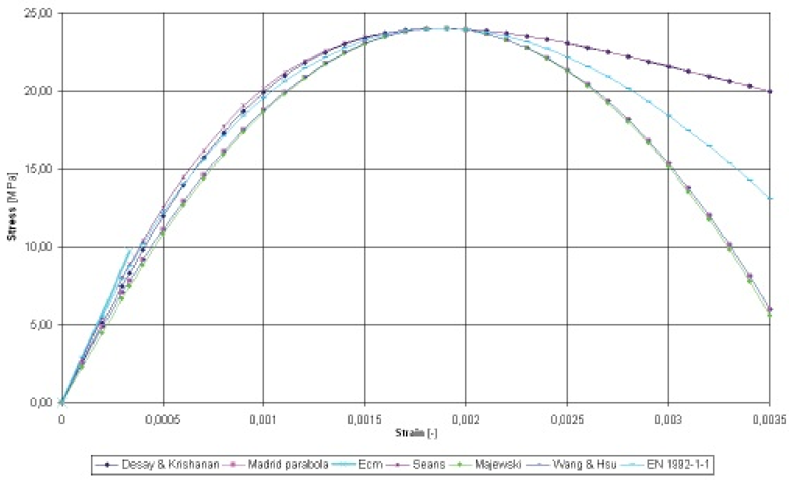

Fig. 12 The comparison of curves σc-εc based on table 2 relations for grade C16/20 concrete

modulus of E_c should artificially be lowered in order to the graph to intersect the correct value f_{cm}. A precise description of relation $\sigma_c - \varepsilon_c$ has been proposed by Sáenz. The function with a 3rd order polynomial in denominator (Table 3) has depended on the variables

$$A = \frac{1}{E_c}, \quad B = \frac{p_3+p_4-2}{p_3 f_{cm}}, \quad C = -\frac{2p_4-1}{p_3 f_{cm}\varepsilon_{c1}}, \quad D = \frac{p_4-1}{p_3 f_{cm}\varepsilon_{c1}}$$
$$P_1 = \frac{\varepsilon_{cu}}{\varepsilon_{c1}}, \quad P_2 = \frac{f_{cm}}{f_{cu}}, \quad P_3 = \frac{E_c\varepsilon_{c1}}{f_{cm}}, \quad P_4 = \frac{P_3(P_2-1)}{(P_1-1)^2} - \frac{1}{P_1} \tag{16}$$

The above notation allows to shape the function graph so that it intersects the points: (ε_{c1}, f_{cm}) and (ε_{cu}, f_{cu}). In this case, the relation proposed by Wang and Hsu is an interesting notation. These are two functions while describing the curve's ascending and descending part. They also include the coefficient ζ that represents the compressive stress of concrete reduction resulted from the locating reinforcing bars in compressed zone. In Fig. 12 ζ=1.0 (no reinforcement taken into account). Adding that Wang and Hsu (2001) relation, Majewski (2003) relation and Madrid parabola almost coincide. The same applies to Desay and Krishanan (Xiao 2000) relation and Sáenz (Sasani 2008) relation, however, in the latter case, the same point (ε_{cu}, f_{cu}) which is followed from the Desay and Krishanan (Xiao 2000) formula has been assumed because a

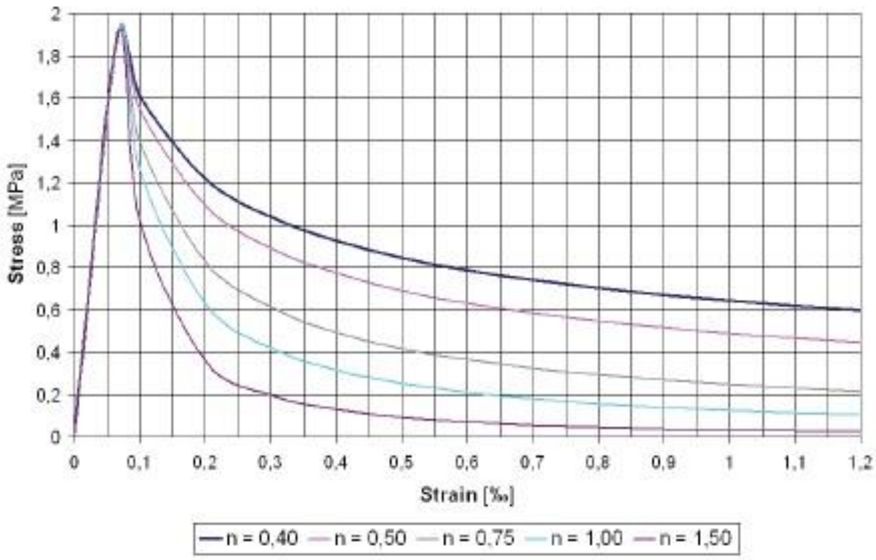

Fig. 13 Modified Wang & Hsu (when) formula for weakening function at tension stiffening for concrete C16/20

lower value of function f_{cu} could be resulted in an improper shape of the curve. The standard relation yields intermediate results. In order to plot the curve $\sigma_t - \varepsilon_t$, the form of weakening function should be defined. Following ABAQUS user-manual (2009), stress can be linearly reduced to 0, thus starting from the moment of reaching the tensile strength to total strain is ten times higher than the moment of reaching f_{ctm}. However, an accurate description of the model function needs to be calibrated with the results predicted for a specific analyzed case.

The proper relation is proposed by Wang and Hsu (2001)

$$\sigma_t = E_c \varepsilon_c \qquad if \quad \varepsilon_t \leq \varepsilon_{cr}$$
$$\sigma_t = f_{cm}\left(\frac{\varepsilon_{cr}}{\varepsilon_t}\right)^{0.4} \qquad if\ \varepsilon_t > \varepsilon_{cr} \tag{17}$$

ε_{cr} = strain at concrete cracking

Since the tension stiffening might considerably affect the results of analysis and the relation that needs calibrating for a given simulation, it is proposed to use the modified Wang and Hsu (2001) formula for the weakening function (Fig. 13)

$$\sigma_t = f_{cm}\left(\frac{\varepsilon_{cr}}{\varepsilon_t}\right)^{n} \qquad if\ \varepsilon_t > \varepsilon_{cr} \tag{18}$$

n = the rate of weakening

As a result, the stress – strain curvatures in CDP model for ABAQUS is defined (Figs. 14 and15). After assembling the instances of model, defining the interactions and suitable boundary supporting conditions, the final model of building has been achieved in ABAQUS (Fig. 16).

3.2 Punching shear occurring and modeling validity

During the modeling process, conditions have been defined align with the occurrence of punching shear. At the end of the analysis, punching shear occurrence is seen according to the obtained deformations of foundation and its bars at the region of axis A and B columns (Figs. 17 and 18). By going through the Figs. 17 and 18, it is obviously determined that the level of deformation at the footing regions of axis A and B's columns in foundation and its bars are highly bigger and this deformation is occurred abrupt. After the visual ensuring of punching shear occurrence in foundation by comparing the deformation values in punched regions between the constructed foundation and the model results (Table 4), it is observed that these values are adequately close to each other and any differences between them are lower than 10%. According to the low difference of deformation values, it is inferable that this building has been correctly modeled and the obtained results of modeling analysis as stress and deformation for foundation frame and bars are adequately valid.

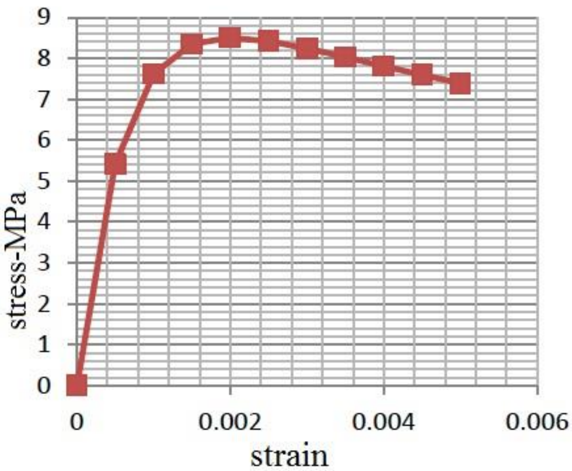

Fig. 14 Foundation's concrete stress-strain curve for uniaxial compressive

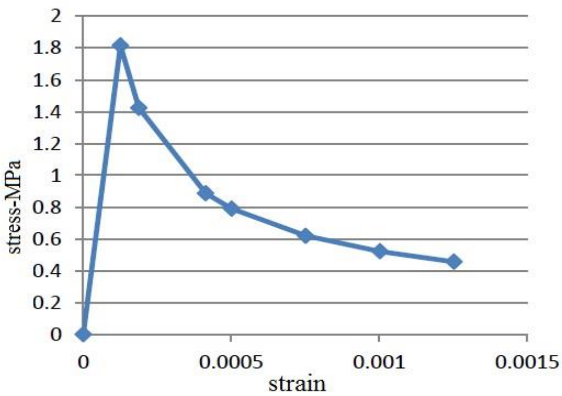

Fig. 15 Foundation's concrete stress – strain for uniaxial tension

Fig. 16 Created model in ABAQUS

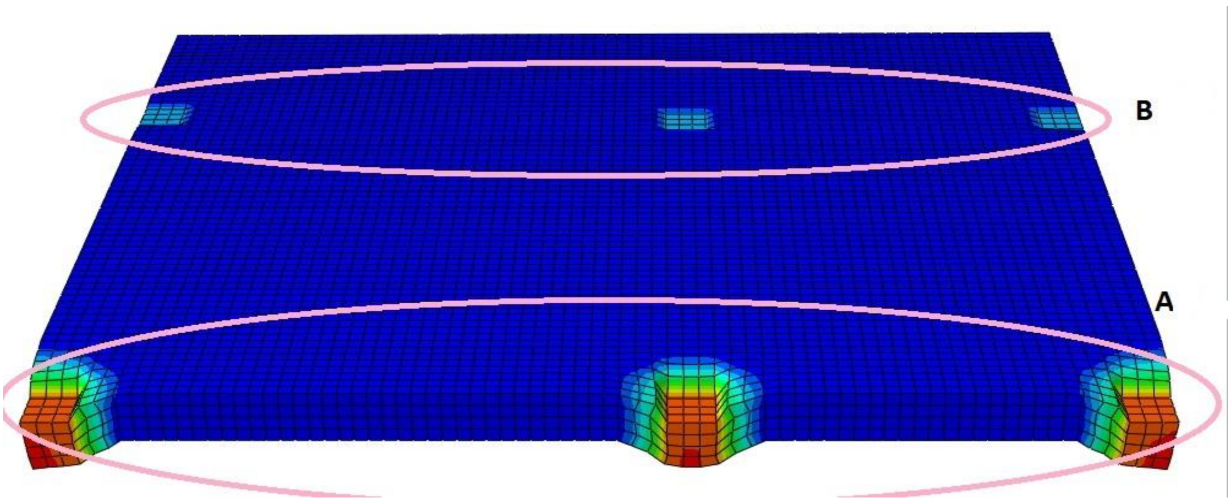

Fig. 17 Punching shear in the concrete of the foundation

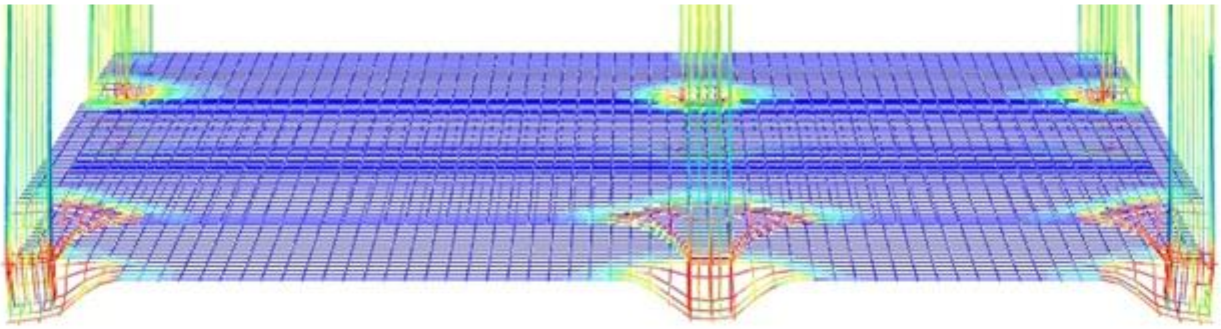

Fig. 18 Deformation of the foundation’s bars due to punching shear in axis A

Table 4. Foundation deformation’s value comparison between model and the building

Column name	Deformation in the constructed foundation (*cm*)	Deformation in the foundation of the model (*cm*)	Difference between deformations (*cm*)	Ration of the deformation’s difference to constructed foundation’s deformation
A - 1	20	18.5	1.5	7.5
A – 2	20	18.7	1.3	6.5
A – 3	20	19	1	5
B – 1	5	4.8	0.2	4
B – 2	5	4.6	0.4	8
B – 3	5	4.6	0.4	8

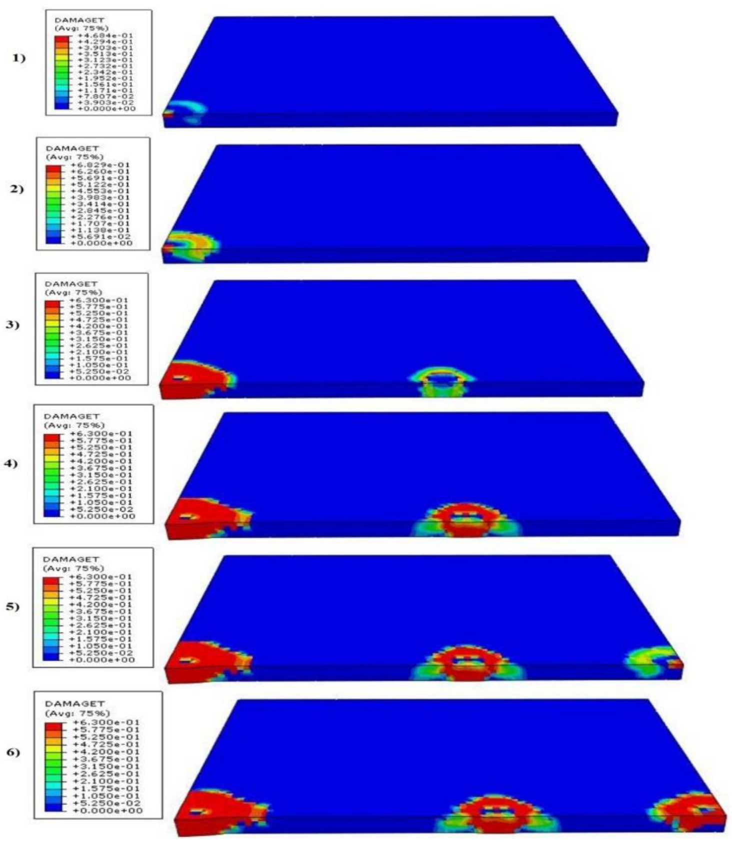

Fig. 19 Foundation’s concrete stress – strain for uniaxial tension

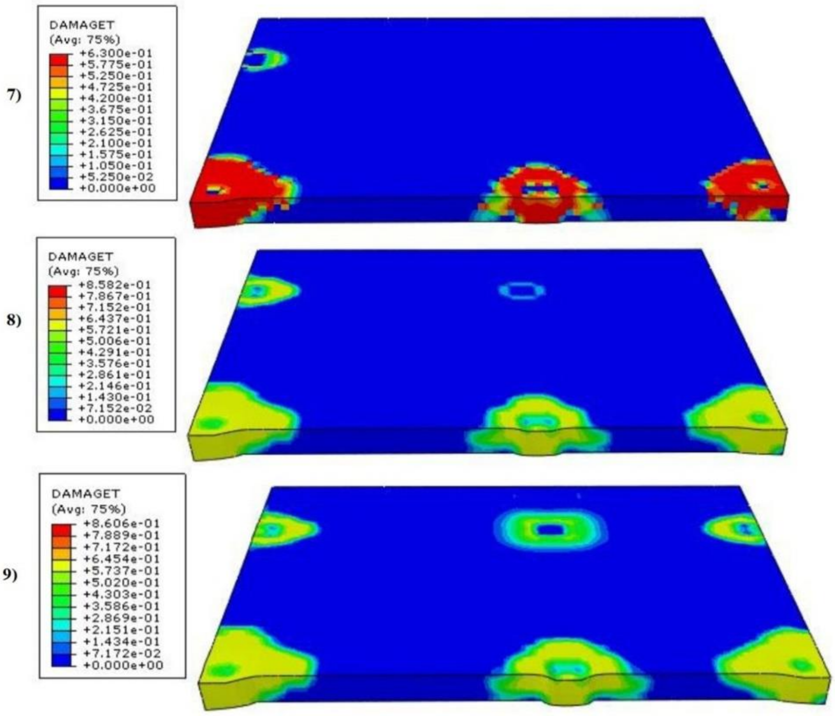

Fig. 19 Continued: The Process of foundation progressive collapse due to punching shear under column A-1 to B-3

Fig. 20 Foundation shear punch under column B-2 in constructed building

3.3 Foundation progressive collapse

By investigating the analysis process, it is obtained that the punching shear occurrence in the regions of 6 columns foots has not been simultaneously happened, which is started from one column foot to another in an intermittent process until it has ultimately been stopped. The fracture progressing process is in a way that the value of stresses in the region of column A-1 foot in foundation has been initially increased and increased the width of cracks. The crack formation has caused a deformation about a few centimeters to happen. By deformation occurrence, some portions of the loads which are tented to carry by column A-1 is transferred to other columns and increased the value of stresses in their foot regions (mostly column A-2 and B-1). The process of stress value increment is continued until the foundation has been punched at the region of column A-2 and some portion of this column’s loads redistributed to others exactly as the column A-1 punched the foundation. The load redistribution which is the result of the foundation shear punch increase the value of the stresses at the foot region of other columns and led them to punch the foundation as well. By yielding the bars of foundation at the region of column A-1 and A-2, the stress value at the region of other columns in foundation is also increased and made the foundation to be consequently punched at the region of column A-3 and B-1 in less time. When the foundation has started to be punched under the column A-3 (increase in widths of the concrete cracks and increase in the stresses values which are transferring to bars), the axis A is weakened to carry the loads and its vertical deformation has been suddenly increased, meaning that the punching shear phenomenon is completed under all three columns of axis A. During the vertical deformation of axis A which is caused by punching shear, transferring of the load from this axis to its side axis (axis B) has been increased and make the foundation to be punched under the column B-1 at first and then at the region of column B-2 and B-3 almost simultaneously. This process of foundation progressive shear punch in the mentioned building has been shown in Fig. 19 by the foundation's concrete damage criteria. In Fig. 20, a punching shear which is occurred under a column of constructed building (pictured in site visit) is shown as an example.

A considerable point about the progressive collapse in the foundation of this building is that the collapsing progress is not reached to all the regions of foundation and almost any progress to the frame (based on stress values in the frame). In fact, the progressive collapse happened in the foundation of building has not caused its falling down while claiming that the frame of building is usable.

4. Stress and displacements

4.1 Foundation stresses

The Punching shear occurrence in foundation under 6 columns while causing big displacements has created some stresses in the foundation, especially under the columns of axis *A* and *B*. The values of stresses in concrete and the bars of foundation (Table 5) has indicated that the loads which are transferred to the foundation by the columns has created stresses in the foundation concrete about its compressive strength and in its bars more than steel yielding strength. These stresses are big enough to cause a complete fracture in the regions' concrete and its separation from other foundation zones. When the foundation concrete has experienced the first cracks, some portions of its stresses are transferred to the cracks region's bars. By growing the crack's widths and continuing of this process, the values of stresses which are transferred to the foundation bars has been also increased. This process has been continued until a peripheral crack in a frustum shape under the columns in foundation is created while separating this region from the other regions of foundation. Separation of these regions' concrete has made the bars to tolerate all the stresses. When the values of the bars stresses exceeds from their yielding strength, this has made a big deformation. In other words, when the stresses of the bars has been increased to their yielding strength, bars try to dissipate the stored energy of these regions by experiencing a big displacement. According to Table 5, it is observed that under the columns of axis *C,* the values of stresses in foundation concrete and bars are less than its compressive strength and steel yielding strength. Therefore, in the regions of axis *C*'s columns, any significant displacement and shear punching phenomenon have not been occurred. Site visiting and reports have stated that any columns of axis *C* has not been punched as well.

4.2 Frame stresses and displacements

The occurrence of punching shear in the foundation of this building can be considered as axisymmetric subsidence for its frame. Axisymmetric subsidence creates inappropriate displacements and stresses in undetermined structures. Punching shear happening in the regions of mentioned columns at the site of building has rotate the building to one side. The rotation and overturning of model has been obtained at the end of the analysis. Indeed, the vertical displacement of axis *A* and *B*'s columns has caused the horizontally shifting of floors (Figs. 21 and 22). In Table 6, every floors horizontally shifted and drifts has been obtained.

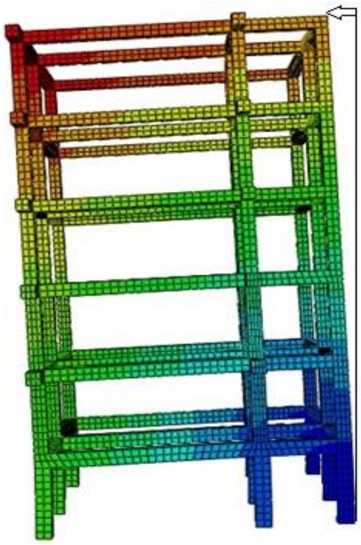

Fig. 21 Frame deformation after foundation shear punch

Table 5 The stresses values in concrete and bars of the foundation under each column

Column name	Stress in the foundation concrete (MPa)	Stress in the bars of the foundation (MPa)
A-1	8.5	353
A-2	8.5	350
A-3	8.5	354
B-1	8.5	324
B-2	8.5	319
B-3	8.5	330
C-1	7.4	101
C-2	7.8	123
C-3	7.6	118

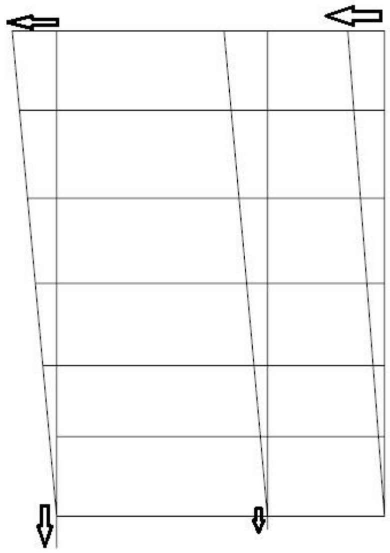

Fig. 22 Rotation of building caused a horizontally floor shifting

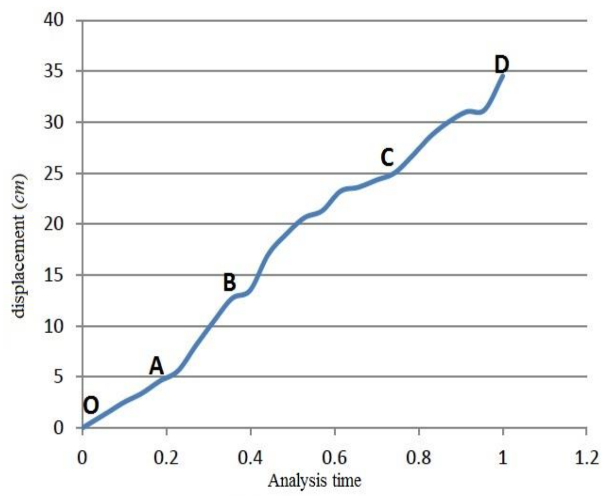

Fig. 23 Horizontal displacement of 5th floor

According to Table 6, the biggest drift has been occurred in the ground floor, meaning that the angle between this floor's columns and beams is changed more than other floors. According to the floors little and near drifts, it is inferable that the angle between the columns and beams of first floor to 5^{th} floor has almost remained unchanged (connections of the beams and columns remained rigid). In this case, after the ground floor, a horizontal displacement of structure is linear (because any length of height equal with the horizontal displacement has been occurred).

The horizontal displacement of 5^{th} floor is shown in a graph (Fig. 23). Thus, the horizontal displacement of 5^{th} floor during the foundation shear punch occurrence can be divided to 4 parts. Due to the uniform and lenient slope, the region between point *O* to point *A* can be considered that the horizontal displacement of floors are related to the first steps of shear punch in the foundation, which increase the stresses and vertical displacement of foundation occurred by the creation of cracks (Fig. 23). Indeed, this region of graph is related to those steps of shear punch phenomenon, showing that the cracks width in the foundation are not too big to transfer considerable stresses to the bars. Obviously, an abrupt slope change has been occurred when the graph reaches to point *A*. In fact, the region between *A* and *B* in Fig. 23 can be related to those steps of shear punch in foundation, in which the width of cracks has been increased and the values of stresses transferred to the bars are raised. This process continues till the concrete in the shear punch regions is completely separated from other parts of the foundation's concrete. In point *B* of the graph, almost the whole stresses under the punched columns is carried by bars. Regarding the region between point *B* to *C* in Fig. 23, the graph goes up with a rather uniform slope and can be related to those steps of shear punch that all the stresses in punch region of foundation are carried by the bars, thus the value of these stresses has been raised. This process of stress increment is continued till the point *C* which can be corresponded to bars yielding. In fact, point *C* is corresponded to the time on which the values of stresses applied to the bars is increased to their yielding stress and after this point the slope of graph is suddenly increased. The region between point *C* to *D* of graph in Fig. 23 has shown a horizontal displacement caused by those steps of shear punch in which the values of stresses exceed the bars yielding strength, thus the bars has experienced big displacements. Finally, in point *D,* the values of displacement(s) stop raising and the stresses applied to the bars are remained in it as residual stresses.

Happening of axisymmetric deformations make stresses in undetermined structures, thus the occurrence of displacements caused by shear punch in the foundation of modeled building has made some stresses in its frame. Based on the stresses values in Table 7, created stresses in concrete and bars caused by frame displacement are not sizable. The concrete stress values in all floors elements are less than the half of frame concrete compressive strength (21 N/m^2) with the exception of ground floor. In fact, the values of stresses in floors 1 to 5 are in a linear elastic limit of concrete based on most codes assumption. The values of stresses obtained from the modeling for grand floor's columns and beams are in magnitude that creates some slight cracks. These cracks in ground floor elements have been confirmed in site visiting reports. Similarly, frame bars stresses has not been exceed from the steel elastic limitation with the exception of ground floor. Based on the values of stresses given in Table 7, created displacement in the frame can't make irreparable damages in it or its performance with trouble.

Therefore, if we could apply an inverse loading in order to resolve the frame displacements without creating any additional stresses (return the rotated frame to its first vertical position), those mentioned frame can be useable for the expectations defined for the building. In case of reusing the building's frame, essential preparation for its foundation should be considered.

Table 6 Floors' displacements values and drifts

Floor name	Horizontal displacement obtained from software (*cm*)	Horizontal displacement in the building (*cm*)	Every floors height (*m*)	Drift %
Ground floor	18.1	-	2.75	6.5
1th floor	19.9	-	3	0.6
2th floor	22.4	-	3	0.83
3th floor	25.8	-	3	1.13
4th floor	29.8	-	3	1.33
5th floor	34.5	36.41	3	1.57

Table 7 Stresses values in frame and its bars

Floor name	The most critical stress value in the columns (*MPa*)	The most critical stress value in the beams (*MPa*)	The most critical stress value in the bars of the columns (*MPa*)	The most critical stress value in the bars of the beams (*MPa*)
Ground floor	18.1	14.3	250	199
1th floor	10.25	12.9	123	102
2th floor	8.76	11.54	71	93
3th floor	8.3	10.14	53.5	70.7
4th floor	8.1	10.3	39.9	51.5
5th floor	8.7	10.2	45.4	61.7

5. Inverse loading, its stresses and displacements

Based on the frame stresses and displacements in Table 7 and the results obtained from the applying an inverse loading to resolve the rotation of frame, it is probably useable as a safe frame. In the second step of model analysis, it applies inverse displacements in a vertical direction to those columns which is punched to the foundation with amplitude exactly equal with their displacements at the end of shear punch phenomenon. In the second step of the analysis, the building's frame has been analyzed under some displacement loads which are applied to resolve the rotation of the frame. Based on Table 8, almost all the horizontal displacements of the frame in Table 6 are resolved by inverse loading and its residual values are negligible. The modified form of frame after the second step of analysis has been shown in Fig. 24. Therefore, the frame overturning is resolved and standing vertically. In Fig. 25, the graph of 5th floor has resolved the horizontal displacement due to the inverse displacement loads to columns. This graph can be divided in two parts 1) point *A* to *B* and 2) point *B* to *C*. Based on smooth slope of graph in first part (1), this region can be related to those steps of the inverse loading that in the yielded bars of foundation has created some deformations to resolve the residual deformations created during the shear punch occurrence. In the region between point *A* and *B* of the graph in Fig. 25, when the inverse loading is applied to the columns, most of it are assigned to resolve the residual deformations of bars and less parts of it are assigned to resolve the horizontal displacement of floors. Therefore, the slope of graph in this region is smooth. When the inverse loads are applied to the columns, the foundation bars tolerate them till to create stresses (caused by the invers load) in the bars about the point *B* reach to their yielding strength.

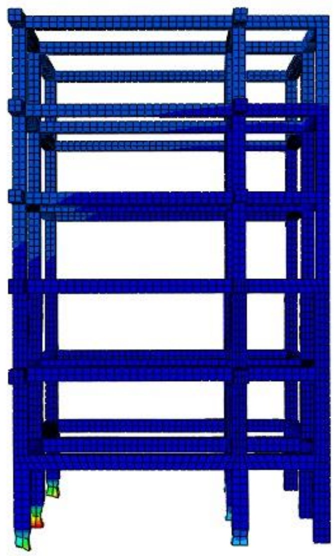

Fig. 24 Deformation of frame after inverse loading

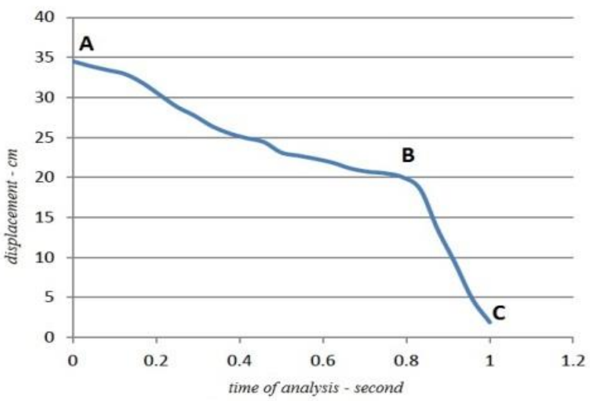

Fig. 25 Resolved deformation of 5th floor during inverse load

Table 8 Residual horizontal displacements of frame after invers loading

Floor name	Horizontal displacement in every floor (*cm*)	Resolved horizontal displacement in every floor (*cm*)	Residual horizontal displacement in every floor (*cm*)
Ground floor	18.1	17.1	1
1th floor	19.9	18.7	1.2
2th floor	22.4	21	1.4
3th floor	25.8	24.2	1.6
4th floor	29.8	28.1	1.7
5th floor	34.5	32.6	1.9

Table 9 The values of stresses in the frame and its bars after inverse loading

Floor name	Maximum stress value in the columns (*MPa*)	Maximum stress value in the beams (*MPa*)	Maximum stress values in the bars of the columns (*MPa*)	Maximum stress values in the bars of the beams (*MPa*)
Ground floor	14.7	12.3	120	79
1th floor	8.1	6.7	83	66
2th floor	6.1	4.6	46	35
3th floor	4.4	3.07	26	18
4th floor	4.4	3.03	23	15
5th floor	4.3	3.6	21	12

During the inverse loading, closure of the cracks in the beams and columns of frame can be another reason for the smooth slope of graph at first part. According to the above descriptions in the second part (point *B* to *C*), after the closure of frame's cracks and foundation's bars yielding, majority of inverse loading efforts has been assigned to resolve the rotation of frame and horizontal displacements of floors. In Table 9, the values of stresses in the frame after an inverse loading, the resolving rotation of frame, horizontal displacements of floors and reaching to an acceptable geometric form for the frame has been presented. By comparing Tables 7 and 9, it is inferable that by applying an inverse load in order to resolve the rotation of frame and horizontal displacements of floors, the stresses of frame has been reduced.

In fact, the factor made these stresses is axisymmetric deformations and by its resolving, the stresses are reduced.

6. Conclusions

Based on the frame and foundation values of stresses and deformations obtained from the modeling analyze, following statements are inferable. By happening of shear punch in the foundation at the regions of six columns followed by the rotation of building to one side, the created stresses in the beams and columns of all floors both in concrete and bars has not exceeded from the material's elastic range except in ground floor. Regarding the values in concrete, the bars of ground floor has exceeded the material's elastic limits, however, they are much less than the concrete's compressive strength and steel' ultimate strength. Despite a rotation occurring in the frame and causing a horizontally shifting of 35 *cm* in 5th floor, the angle of beams and columns in all floors has not been changed and the connections between these elements are stayed rigid except in ground floor. In ground floor, by creation of cracks in the connection regions of beams and columns which are punched, these connections has not behaved rigid.

1) The values of stresses in concrete and the bars of foundation in the regions of punched columns are highly exceeded from the concrete's compressive strength and the bar's yielding strength while remained as residual stresses in the bars. Thus, according to the high values of residual stresses in the foundation's materials, foundation can't be reusable.
2) The occurrence of shear punch in the regions of six column of construction has not been happened at ones, but is a progressive collapse which is started from a point to another and finally stopped, thus the building has not been totally destructed.

By applying inverse loading to the structure, almost all the horizontal displacements of the floors are resolved and the building is stood vertically. By resolving the created horizontal deformations in the structure, floors stresses values have been considerably reduced, thus the frame of the building is useable again after the inverse loading.

References

Davoodnabi, S.M., Mirhosseini, S.M. and Shariati, M. (2019), "Behavior of steel-concrete composite beam using angle shear connectors at fire condition", *Steel Compos. Struct.*, **30**(2), 141-147.DOI: https://doi.org/10.12989/scs.2019.30.2.141.

Hosseinpour, E., Baharom, S., Badaruzzaman, W.H.W., Shariati, M. and Jalali, A. (2018), "Direct shear behavior of concrete filled hollow steel tube shear connector for slim-floor steel beams", *Steel Compos. Struct*., **26**(4), 485-499. https://doi.org/10.12989/scs.2018.26.4.485.

Ismail, M., Shariati, M., Abdul Awal, A.S.M., Chiong, C.E., Sadeghipour Chahnasir, E., Porbar, A., Heydari, A. and khorami, M. (2018), "Strengthening of bolted shear joints in industrialized ferrocement construction", *Steel Compos. Struct*., **28**(6), 681-690. https://doi.org/10.12989/scs.2018.28.6.681.

Khorramian, K., Maleki, S., Shariati, M. and Ramli Sulong, N.H. (2016), "Behavior of Tilted Angle Shear Connectors (vol 10, e0144288, 2015)", *PLoS One*, **11**(2).

Li, D., Toghroli, A., Shariati, M., Sajedi, F., Bui, D.T., Kianmehr, P., Mohamad, E.T. and Khorami, M. (2019), "Application of polymer, silica-fume and crushed rubber in the production of Pervious concrete", *Smart Struct. Syst*., **23**(2), 207-214. https://doi.org/10.12989/sss.2019.23.2.207.

Li, K., Wang, X.L., Cao, S.Y. and Chen, Q.P. (2015), "Fatigue behavior of concrete beams reinforced with HRBF500 steel bars", *Struct. Eng. Mech*., **53**(2), 311-324. https://doi.org/10.12989/sem.2015.53.2.311.

Luo, Z., Sinaei, H., Ibrahim, Z., Shariati, M., Jumaat, Z., Wakil, K., Pham, B.T., Mohamad, E.T. and Khorami, M. (2019), "Computational and experimental analysis of beam to column joints reinforced with CFRP plates", *Steel Compos. Struct*., **30**(3), 271-280. http://dx.doi.org/10.12989/scs.2019.30.3.271.

Mohammadhassani, M., Akib, S., Shariati, M., Suhatril, M. and Arabnejad Khanouki, M.M. (2014), "An experimental study on the failure modes of high strength concrete beams with particular references to variation of the tensile reinforcement ratio", *Eng. Fail. Anal*., **41**, 73-80. https://doi.org/10.1016/j.engfailanal.2013.08.014.

Naghipour, M., Yousofizinsaz, G. and Shariati, M. (2020). "Experimental study on axial compressive behavior of welded built-up CFT stub columns made by cold-formed sections with different welding lines", *Steel Compos. Struct*., **34**(3), 347. https://doi.org/10.12989/scs.2020.34.3.347.

Nasrollahi, S., Maleki, S., Shariati, M., Marto, A. and Khorami, M. (2018), "Investigation of pipe shear connectors using push out test", S *Steel Compos. Struct*., **27**(5), 537-543. http://dx.doi.org/10.12989/scs.2018.27.5.537.

Nosrati, A., Zandi, Y., Shariati, M., Khademi, K., Darvishnezhad Aliabad, M., Marto, A., Mu'azu, M., Ghanbari, E., Mandizadeh, M.B. and Shariati, A. (2018), "Portland cement structure and its major oxides and fineness", *Smart Struct. Syst*., **22**(4), 425-432. https://doi.org/10.12989/sss.2018.22.4.425.

Paknahad, M., Shariati, M., Sedghi, Y., Bazzaz, M. and Khorami, M. (2018), "Shear capacity equation for channel shear connectors in steel-concrete composite beams", *Steel Compos. Struct*., **28**(4), 483-494. http://dx.doi.org/10.12989/scs.2018.28.4.483.

Sajedi, F. and Shariati, M. (2019), "Behavior study of NC and HSC RCCs confined by GRP casing and CFRP wrapping", *Steel Compos. Struct*., **30**(5), 417-432. https://doi.org/10.12989/scs.2019.30.5.417.

Shahabi, S., Ramli Sulong, N. H., Shariati, M. and Shah, S. (2016), "Performance of shear connectors at elevated temperatures-A review", *Steel Compos. Struct*., **20**(1), 185-203. https://doi.org/10.12989/scs.2016.20.1.185.

Shariati, M. (2013), Behaviour of C-shaped Shear Connectors in Stell Concrete Composite Beams, Jabatan Kejuruteraan Awam, Fakulti Kejuruteraan, Universiti Malaya.

Shariati, M., Heyrati, A., Zandi, Y., Laka, H., Toghroli, A., Kianmehr, P., Safa, M., Salih, M.N. and Poi-Ngian, S. (2019a), "Application of waste tire rubber aggregate in porous concrete", *Smart Struct. Syst*., **24**(4), 553-566. https://doi.org/10.12989/sss.2019.24.4.553.

Shariati, M., Rafiei, S., Zandi, Y., Fooladvand, R., Gharehaghaj, B., Shariat, A., Trung, N.T., Salih, M.N., Mehrabi, P. and Poi-Ngian, S. (2019b), "Experimental investigation on the effect of cementitious materials on fresh and mechanical properties of self-consolidating concrete", *Adv. Concrete Constr*., **8**(3), 225-237. https://doi.org/10.12989/acc.2019.8.3.225.

Shariati, M., Ramli Sulong, N.H., Arabnejad Khanouki, M.M. and Shariati, A. (2011), "Experimental and numerical investigations of channel shear connectors in high strength concrete", *Proceedings of the 2011 world congress on advances in structural engineering and mechanics (ASEM'11+)*.

Shariati, M., Ramli Sulong, N.H., Suhatril, M., Shariati, A., Arabnejad Khanouki, M.M. and Sinaei, H. (2012), "Fatigue energy dissipation and failure analysis of channel shear connector embedded in the lightweight aggregate concrete in composite bridge girders", *Proceedings of the 5th International Conference on Engineering Failure Analysis*, 1-4 July 2012, Hilton Hotel, The Hague, The Netherlands.

Shariati, M., Toghroli, A., Jalali, A. and Ibrahim, Z. (2017), "Assessment of stiffened angle shear connector under monotonic and fully reversed cyclic loading", *Proceedings of the 5th International Conference on Advances in Civil, Structural and Mechanical Engineering-CSM 2017*.

Sinaei, H., Jumaat, M.Z. and Shariati, M. (2011), "Numerical investigation on exterior reinforced concrete Beam-Column joint strengthened by composite fiber reinforced polymer (CFRP)", *Int. J. Phys. Sci*., **6**(28), 6572-6579.

Suhatril, M., Osman, N., Sari, P.A., Shariati, M. and Marto, A. (2019), "Significance of surface eco-protection techniques for cohesive soils slope in Selangor, Malaysia", *Geotech. Geological Eng*., **37**(3), 2007-2014.

Tahmasbi, F., Maleki, S., Shariati, M., Ramli Sulong, N.H. and Tahir, M.M. (2016), "Shear capacity of C-shaped and L-shaped angle shear connectors", *PLoS One*, **11**(8), e0156989.DOI: https://doi.org/10.1371/journal.pone.0156989.

Toghroli, A., Shariati, M., Karim, M.R. and Ibrahim, Z. (2017), "Investigation on composite polymer and silica fume–rubber aggregate pervious concrete", *Proceedings of the 5th* I*nternational Conference on Advances in Civil, Structural and Mechanical Engineering* - *CSM 2017*, Zurich, Switzerland.

Toghroli, A., Shariati, M., Sajedi, F., Ibrahim, Z., Koting, S., Mohamad, E.T. and Khorami, M. (2018), "A review on pavement porous concrete using recycled waste materials", *Smart Struct. Syst*., **22**(4), 433-440. https://doi.org/10.12989/sss.2018.22.4.433.

Trung, N.T., Alemi, N., Haido, J.H., Shariati, M., Baradaran, S. and Yousif, S.T. (2019), "Reduction of cement consumption by producing smart green concretes with natural zeolites", *Smart Struct. Syst*., **24**(3), 415-425. https://doi.org/10.12989/sss.2019.24.3.415.

Wei, X., Shariati, M., Zandi, Y., Pei, S., Jin, Z., Gharachurlu, S., Abdullahi, M.M., Tahir, M.M. and Khorami, M. (2018), "Distribution of shear force in perforated shear connectors", *Steel Compos. Struct*., **27**(3), 389-399. http://dx.doi.org/10.12989/scs.2018.27.3.389.

Willam, K.J. (1975), "Constitutive model for the triaxial behaviour of concrete", Proc. Intl. Assoc. Bridge Structl. Engrs, **19**, 1-30.

Xie, Q., Sinaei, H., Shariati, M., Khorami, M., Mohamad, E.T. and Bui, D.T. (2019), "An experimental study on the effect of CFRP on behavior of reinforce concrete beam column connections", *Steel Compos. Struct*., **30**(5), 433-441. https://doi.org/10.12989/scs.2019.30.5.433.

Ziaei-Nia, A., Shariati, M. and Salehabadi, E. (2018), "Dynamic mix design optimization of high-performance concrete", *Steel Compos. Struct*., **29**(1), 67-75. https://doi.org/10.12989/scs.2018.29.1.067.

CC